Analysis of percent density estimates from digital breast tomosynthesis projection images

Predrag R. Bakic*, Despina Kontos, Cuiping Zhang, Martin J. Yaffe[1], Andrew D.A. Maidment
Department of Radiology, University of Pennsylvania, 3400 Spruce Street, Philadelphia, PA 19104
[1]Imaging Research, Sunnybrook Health Sciences Centre,
2075 Bayview Avenue Toronto, Ontario, Canada M4N 3M5

ABSTRACT

Women with dense breasts have an increased risk of breast cancer. Breast density is typically measured as the percent density (PD), the percentage of non-fatty (*i.e.*, dense) tissue in breast images. Mammographic PD estimates vary, in part, due to the projective nature of mammograms. Digital breast tomosynthesis (DBT) is a novel radiographic method in which 3D images of the breast are reconstructed from a small number of projection (source) images, acquired at different positions of the x-ray focus. DBT provides superior visualization of breast tissue and has improved sensitivity and specificity as compared to mammography. Our long-term goal is to test the hypothesis that PD obtained from DBT is superior in estimating cancer risk compared with other modalities. As a first step, we have analyzed the PD estimates from DBT source projections since the results would be independent of the reconstruction method. We estimated PD from MLO mammograms (PD_M) and from individual DBT projections (PD_T). We observed good agreement between PD_M and PD_T from the central projection images of 40 women. This suggests that variations in breast positioning, dose, and scatter between mammography and DBT do not negatively affect PD estimation. The PD_T estimated from individual DBT projections of nine women varied with the angle between the projections. This variation is caused by the 3D arrangement of the breast dense tissue and the acquisition geometry.

Keywords: Methods: Quantitative image analysis, Effect of physical imaging parameters; Modalities: Mammography, Digital breast tomosynthesis; Diagnostic Task: Risk assessment.

1. INTRODUCTION

Women with dense breasts have an increased risk of breast cancer.[1-11] The ability to estimate breast cancer risk is of great importance since it may allow customization of breast cancer detection and treatment, especially for patients at high risk of breast cancer. It is hypothesized that by estimating breast density one can estimate cancer risk. The most commonly used description of breast density is the American College of Radiology standardized four-point classification scheme, Breast Imaging Reporting and Data System.[12] While the BI-RADS classification represents a qualitative description, a typically used quantitative measure of breast density is the percent density (PD), the percentage of non-fatty (*i.e.*, dense) tissue in breast images.

Mammographic PD estimates vary, in part, due to the projective nature of mammograms. Digital breast tomosynthesis (DBT) is a radiographic method in which images of parallel slices of the breast are reconstructed from a small number of projection (source) images, acquired at different positions of the x-ray focus.[13, 14] DBT provides superior tissue visualization and has improved sensitivity and specificity compared to mammography.[15, 16]

Our long-term goal is to test the hypothesis that PD obtained from DBT is superior in estimating cancer risk compared with mammography. As a first step, we have analyzed the PD estimates from DBT source projections. Analysis of projection images has value as it is independent of DBT reconstruction algorithms. Our focus was to evaluate the effects of differences in acquisition parameters between mammography and DBT on PD estimation. DBT projections are acquired using breast positioning similar to an MLO mammographic view; however, the two modalities differ in the amount of breast compression, amount of scatter, and radiation dose. In addition, in DBT, multiple projections of the breast are acquired at different angles. To evaluate the effects of the differences in acquisition parameters, we performed

* Predrag.Bakic@uphs.upenn.edu; Phone: 215 746 8758; Fax: 215 746 8764

Medical Imaging 2007: Computer-Aided Diagnosis, edited by Maryellen L. Giger, Nico Karssemeijer,
Proc. of SPIE Vol. 6514, 651424, (2007) · 1605-7422/07/$18 · doi: 10.1117/12.713855

two studies. In the first study, we compared PD estimates from the MLO mammograms and central DBT projections. In the second study we tested the effect of varying the x-ray tube angle by comparing the PD estimates from individual DBT projections.

2. MATERIALS AND METHODS

2.1 Acquisition of clinical mammograms and DBT images

To date we have acquired DBT images of 52 women as a part of a clinical evaluation of multimodality breast imaging at the University of Pennsylvania.[14] Each women in the study also had a digital mammogram. The DBT projections have been acquired using a Senographe 2000D (General Electric Medical Systems, Milwaukee, WI) digital mammography machine, modified to allow the x-ray focus to be positioned at nine angles, each 6.25° apart; covering a total angular range of [-25°,25°]. The nine DBT projections were taken using the same total dose as a standard 2-view mammographic exam and a slightly lower amount of compression. Figure 1 shows an example of clinical images used in this study.

This multimodality breast imaging study included volunteers with a high risk of breast cancer as computed by the Gail[17] and Claus[18] models, women referred to biopsy, and follow-up cancer cases. The clinical DBT images were acquired from the latter two groups. We have selected digital mammograms and DBT images from 40 women (mean age 51.4 years; range 31-80). We estimated PD from the breast contralateral to any finding, since the presence of a lesion could erroneously increase the PD estimate. Twelve women were excluded from our analysis. We excluded women with bilateral lesions and those for whom a unilateral study was performed. Women with breast implants were also excluded. The clinical images were acquired in the period between September 2004 and April 2005. The average lifetime Gail risk value for the population of 40 patients was 10.78% (range 1.8-30.3%).

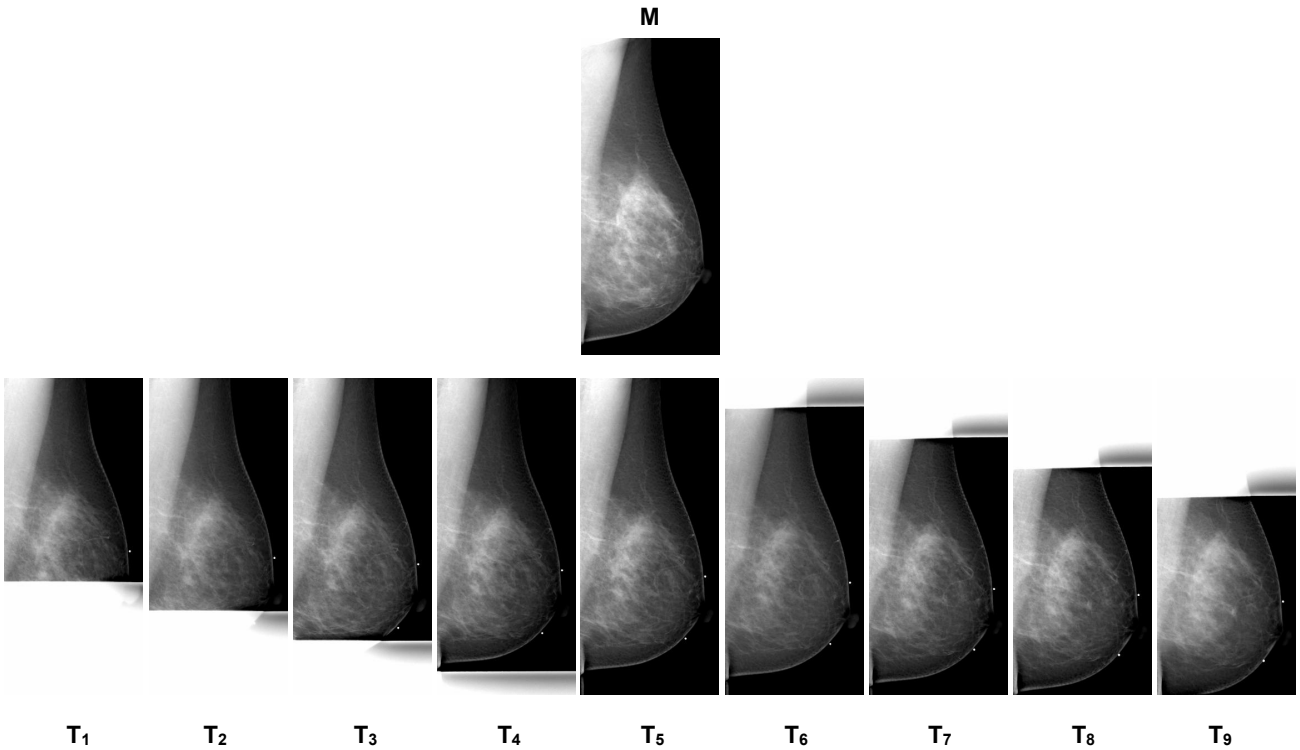

Figure 1: An example of a clinical set of images used for PD estimation in this study. PD estimate is computed from a clinical MLO mammogram (M) and compared with the PD estimated from DBT projection images (T_1-T_9) acquired with different positions of the x-ray focus.

2.2 Estimation of breast PD from clinical breast images

We have estimated PD from DBT projections using Cumulus, a software package developed at the University of Toronto.[5, 19] This software package provides the user with the ability to exclude a region of the breast from PD

estimation (e.g., the pectoral muscle region). The PD estimate is then computed as the ratio between the area within the manually thresholded region representing breast dense tissue and the area within the manually thresholded breast outline.[19] The Cumulus package has been widely validated.[20-27] Alternative methods for estimating PD from clinical mammograms have also been reported.[28, 29]

2.3 Correlation between PD estimated from MLO mammograms and central DBT projections

We have compared mammographic PD estimates (PD_M) and DBT PD estimates (PD_T) from the central DBT projections of the same breast. The PD_M and central projection PD_T values were compared by calculating their Pearson correlation coefficient and by calculating the slope and intercept of their linear regression.

Linear regression of the PD_M and PD_T values is formulated as: $(PD_T)_{LR} = S \cdot PD_M + I$, where S and I represent the linear regression slope and intercept, respectively, and are computed using the following equations:

$$S = \frac{\sum (PD_M \cdot PD_T) - \left(\sum PD_M\right)\cdot\left(\sum PD_T\right)/N}{\sum (PD_M)^2 - \left(\sum PD_T\right)^2 / N}, \text{ and } I = E(PD_T) - b \cdot E(PD_T), \quad (1)$$

where average values $E(PD_M)$ and $E(PD_T)$ have been computed over N selected cases.

The Pearson correlation coefficient r is defined as:

$$r = \frac{\sum (PD_M \cdot PD_T)}{\sqrt{\left(\sum {PD_M}^2\right)\left(\sum {PD_T}^2\right)}}. \quad (2)$$

The summation in Equations (1) and (2) is computed over N selected cases.

2.4 Correlation between PD estimates from individual DBT projections

Availability of clinical DBT projection images acquired at different angles of the x-ray tube, offers a unique opportunity to analyze the dependence of PD estimation on acquisition angle. We tested the angular dependence by computing the average values and the standard deviation (SD) of PD_T estimates for individual DBT projections taken with a given tube angle. We also computed the average Pearson correlation coefficient between individual PD_T estimates of DBT projections acquired at a given angular separation and between PD_T of the central DBT projection and PD_T of DBT projections acquired at a given angular distance from the central projection.

3. RESULTS

3.1 Comparison of PD_M and central projection PD_T

Figure 2 shows a scatter plot and the linear regression of PD computed from the central DBT projections and the corresponding MLO mammograms of 40 women. The Pearson coefficient of correlation between the PD_M and the central projection PD_T values is equal to 0.90, and the slope and intercept values of the linear regression are equal to 1.06 and 1.65%, respectively.

In order to test the reproducibility of the observers, we calculated the intra-observer variations of the PD estimates obtained using Cumulus for a subset of 9 women. Figure 3 compares the results of the reproducibility studies for PD_M values (left) and the projection PD_T values (right). The intra-observer Pearson correlation coefficient is equal to 0.92 for PD_M and 0.94 for the central projection PD_T. The slope values of the linear regression are equal to 0.92 for PD_M and 0.94 for PD_T, and the intercept values are equal to 6.61% for PD_M and 2.05% for PD_T.

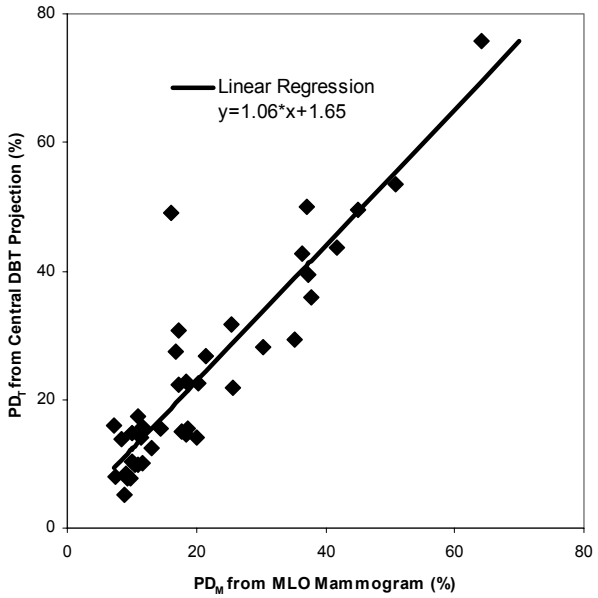

Figure 2: Correlation between PD estimates from mammograms and central DBT projections. Scatter plot of PD estimates from clinical mammograms (PD_M) and from central DBT projections (PD_T), obtained from contralateral breasts of 40 women. The central DBT projection is acquired with the same position of the x-ray focus as the corresponding MLO mammogram. Plotted is also the linear regression of the central projection PD_T values as a function of the PD_M values. The corresponding Pearson correlation coefficient is equal to 0.90.

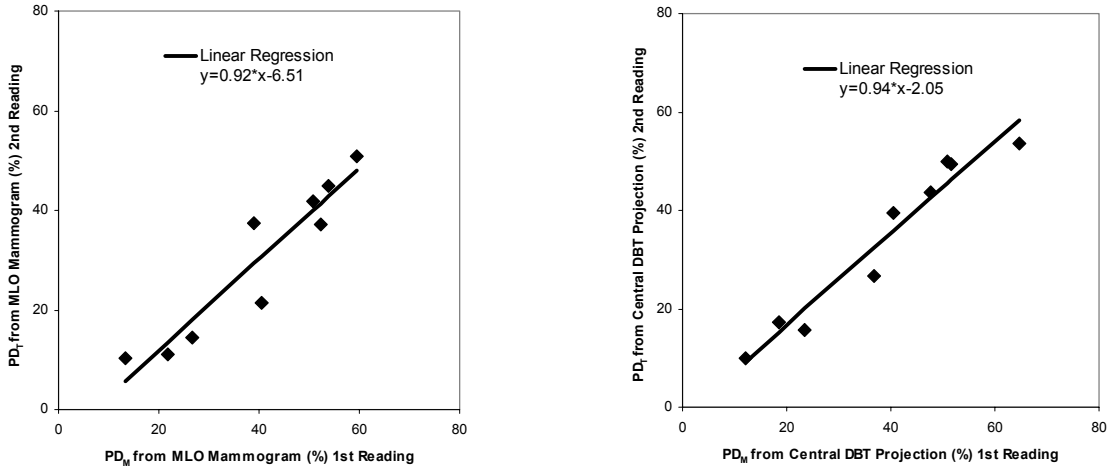

Figure 3: Intra-observer variation. Scatter plot of mammographic PD_M estimates (left) and central DBT projection PD_T estimates (right) from two repeated studies of a subset of clinical images from 9 women. The DBT data and the corresponding mammograms were obtained from the contralateral breasts of 9 women. Plotted are also the intra-observer linear regressions of the PD_M and PD_T values. The Pearson correlation coefficients are equal to 0.92 for PD_M and 0.94 for PD_T.

3.2 Comparison of PD_T from individual DBT projections

We have evaluated the dependence of PD on acquisition angle by comparing the PD_T values calculated for each of the nine DBT projection angles; specifically, we computed the mean and SD of the PD at each DBT angle, and the correlation of PD estimates between different DBT angles. Figure 4 shows the mean and SD of the PD_T estimates for nine women as a function of DBT projection angle.

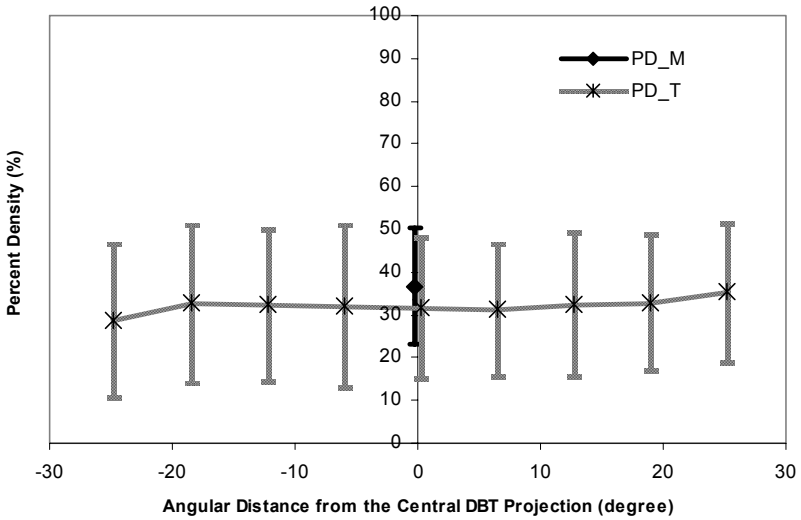

Figure 4: PD_T estimates from individual DBT projections. Plotted are the mean and standard deviation (SD) of the PD_T values for nine women (grey line) as a function of angle. Also, shown is the mean and SD of PD_M for these women (black line). Error bars show ± one SD.

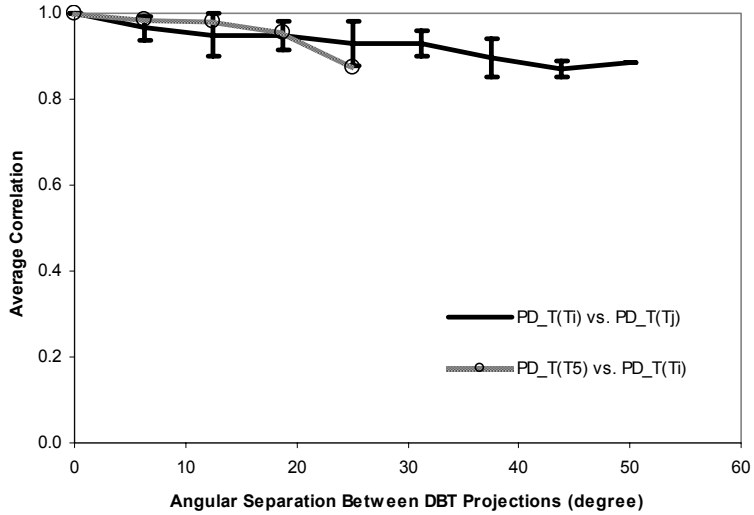

Figure 5: Correlation between PD estimates from mammograms and individual DBT projections. Plotted are the mean and SD of the Pearson correlation coefficients between PD estimates from individual DBT projections acquired at a given angular separation (black line). Also, shown are the average values of the Pearson correlation coefficients between PDt of the central DBT projection and PDt at a given angular separation (grey line). Error bars, when shown, are equal to ± one SD.

Figure 5 shows the average values of the Pearson correlation coefficients between PD_T for DBT projections which are separated by the same angular distance (black line). The average correlations were computed as follows. We first computed the Pearson correlation between any two vectors of PD_T values, corresponding to DBT projections separated by the same angle. (The vector elements are the PD_T values for different women.) For example, the average correlation value for an angular distance of 6.25° was obtained by averaging the Pearson correlations corresponding to eight pairs of DBT projections, each pair separated by 6.25° (*i.e.*, T_1 and T_2, T_2 and T_3, ..., T_8 and T_9; see Figure 1). Similarly, the average correlation value for the angular distance of 12.5° was obtained by averaging the Pearson correlation coefficients corresponding to seven pairs of projections each 12.5° apart (*i.e.*, T_1 and T_3, T_2 and T_4, ..., T_7 and T_9). This procedure was repeated for all angular separations.

We have also computed the corresponding SD values for each angular separation. Error bars in Figure 5 (black line) show ± one SD. Note that the average correlation value for an angular separation of 50° was computed using the Pearson correlation for a single pair of projections T_1 and T_9 and that the average correlation for the zero separation was set to 1 by default. Thus, the SD values for angular separations of 0° and 50° are not shown.

Figure 5 also shows the average values of the Pearson correlations between the central projection PD_T and PD_T's from individual DBT projections acquired at a given angular distance from the central projection (grey line). Error bars show ± one SD.

4. DISCUSSION

4.1 Effects of differences in acquisition parameters between mammography and DBT on PD estimation

It can be seen from Figure 2 that there is good agreement between PD_M and the central projection PD_T. These results suggest that the differences in acquisition parameters (*i.e.*, differences in the amount of compression, radiation dose, and scatter, and variation in positioning between mammography and DBT) do not significantly influence PD estimation. These result are also supported by studies published in the literature of PD estimates obtained using very low radiation dose[30] and with variation in acquisition parameters.

4.2 Angular dependence of PD_T estimates

Figure 4 shows that the PD_T does not vary significantly with acquisition angle. We also observed that the SD of PD_T, computed over all DBT angles, for each individual woman is very low (range 1%-7%). Although the observed variations were small, we were concerned that the changes in collimation as a function of angle would lead to a bias in our results. Note that a portion of each projection image is occluded by the collimator (see Figure 1). This occurs because the fulcrum of the x-ray tube rotation does not coincide with the position of the breast (see Figure 6).

We performed two additional studies to elucidate the effects of the collimation. First, we masked the central projection image to match the collimation for each DBT projection. We then calculated the difference in PD_T estimate for the image acquired at that angle and the central projection image masked according to the collimation at that angle.

Figure 7 (upper graph) shows the mean and SD of the difference between PD_T and the PD of the central projection image masked to match the collimation at a given angle. Error bars show ± one SD. For comparison, we show the SD of the PD_T of the central projection on the same graph. It can be seen that the SD of the difference between the projection PD_T and the PD_T from the masked central projection are 2-6 times smaller than the SD of the individual projection PD_T. This suggest that PD_T values from the masked central projection are highly correlated with the PD_T values from individual projection images.

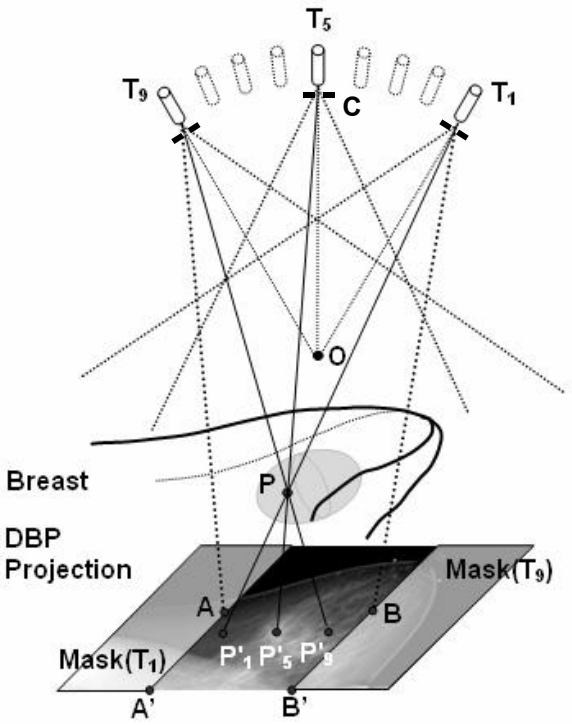

Figure 6: Non-uniform collimation observed during DBT acquisition using our imaging system. The x-ray tube is moved along an arc of (-25°,25°) during the acquisition of DBT projection images (T_1-T_9). Consequently, as the x-ray tube angle changes, the projection onto the detector of a point, P, within the breast will also change; the black lines in the figure illustrate such a projection trajectory. In our imaging system, the center of the tube rotation (O) is outside the breast; gray solid lines indicate x-ray trajectories through the center of tube rotation for various tube angles. At acute angles, the x-ray collimator (C) enters the field of view; as a result regions of the breast are occluded. Dashed lines indicate the borders of the field of view for various tube angles.

Second, we applied the same mask to each projection image and calculated the PD_T. We used a mask formed by the union of the collimated regions of the breast. As a result, only the same central portion of each projection image was used to estimate PD_T.

It can be seen from Figure 7 (lower graph) that there are differences between the PD_T estimated at a given angle. A possible cause of these differences is that, due to the projection acquisition geometry, there is motion of the fibroglandular (*i.e.*, dense) tissue region in one DBT projection relative to the other (see Figure 6). In combination with the applied masking, this motion results in different amounts of dense tissue being visible in the central image portion and hence used to estimate PD_T. This effect is illustrated in Figure 8. Without collimation, the whole area of the dense tissue will be visualized in each projection, thus reducing the effects of the projective geometry on PD estimation.

Our department has recently installed a new breast imaging system, Senographe DS (General Electric Medical Systems, Milwaukee, WI), which is optimized for DBT acquisition. The collimation effects, described in this section, have been eliminated in the new system.

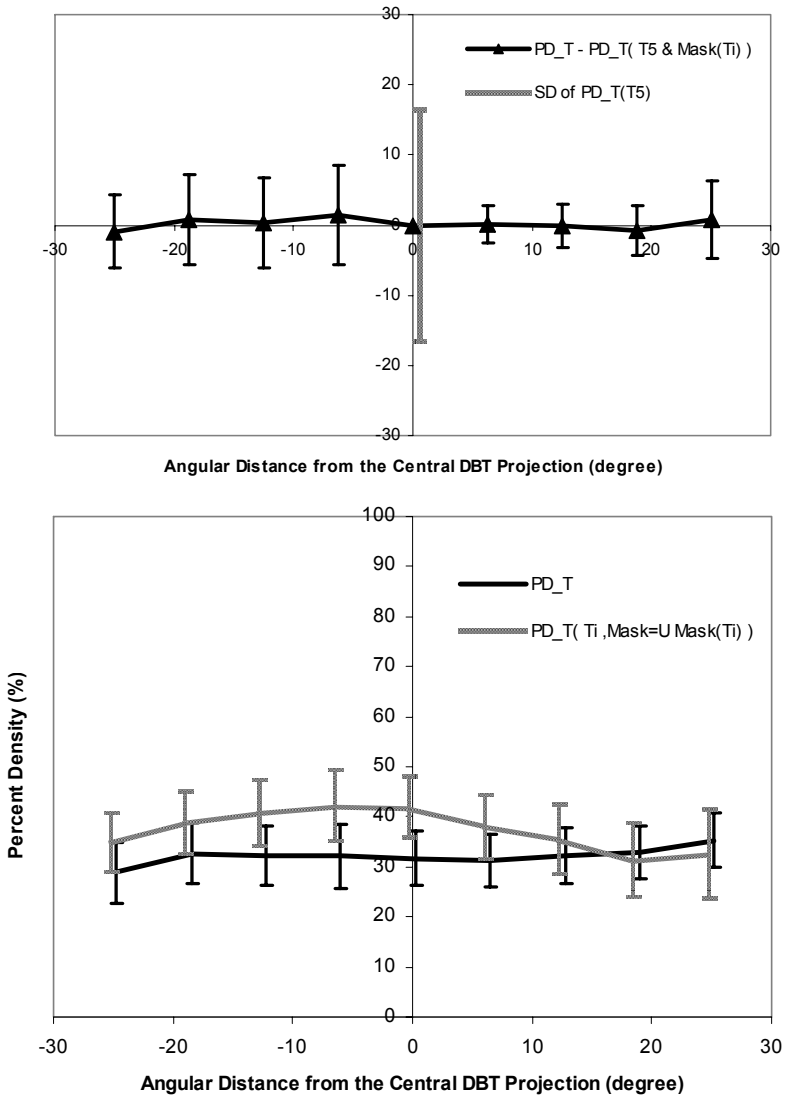

Figure 7: Analysis of the effects of non-uniform collimation on PD estimation from DBT projections. (Upper graph) Plotted are the mean and SD of the differences between PD_T of individual projections and PD_T of the central projection masked to match the collimation for each DBT projection (black line). Solid error bars show ± one SD. Also, plotted is an error bar corresponding to ± one SD for the central projection PD_T (grey line). (Lower graph) Plotted are the mean and SD of PD_T of individual DBT projection (black line) and the PD_T estimated when the same mask is applied to each projection image (grey line). The mask was formed by the union of the collimated regions in all projections. Error bars show ± one standard error.

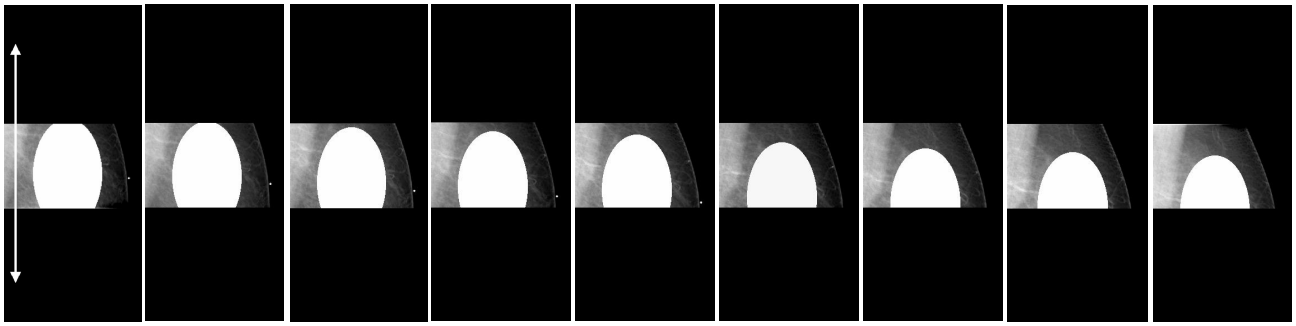

T_1 T_2 T_3 T_4 T_5 T_6 T_7 T_8 T_9

Figure 8: Changes in visualized breast anatomy in the sequence of nine DBT projection images (T1-T9). We modified DBT projection images from Figure 1, using the mask formed by the union of all collimated regions in the DBT projection images (black). The PD_T was calculated in all the masked images. (Arrows indicate the direction of the x-ray tube motion. White elliptical overlays in T1-T9 indicate approximate positions of dense tissue regions in DBT projections.)

5. CONCLUSIONS

We have estimated the PD from DBT projections (PD_T) and mammograms (PD_M) for 40 women. We have computed the Pearson correlation coefficients and the linear regression between PD_M and PD_T. There is little variation in PD_M and the PD_T of the central DBT projection, suggesting that the differences in acquisition parameters between mammography and DBT do not affect PD estimation. In addition, we analyzed the angular dependence of PD_T for 9 women. The obtained results do not show a significant variation with acquisition angle. We did observe small variations due to the projective geometry and the variation in collimation as a function of angle. To the best of our knowledge, this study represents the first analysis of the variation in 2D estimates of the breast percent density as a function of the projection angle.

ACKNOWLEDGMENT

This work was supported by Susan G. Komen Breast Cancer Foundation Research Grant BCTR133506 and by National Institutes of Health/National Cancer Institute Program Project Grant P01-CA85484. The authors are grateful to Dr. Ann-Katherine Carton for her help with the acquisition of digital breast tomosynthesis images.

REFERENCES

1. Boyd NF, Byng JW, Jong RA, et al. Quantitative classification of mammographic densities and breast cancer risk: results from the Canadian National Breast Screening Study. *Journal of the National Cancer Institute.* 1995;87(9):670-675.

2. Boyd NF, Guo H, Martin LJ, et al. Mammographic density and the risk and detection of breast cancer. *NEJM.* 2007;356(3):227-236.

3. Boyd NF, Lockwood GA, Byng JW, Tritchler DL, Yaffe MJ. Mammographic densities and breast cancer risk. *Cancer Epidemiology, Biomarkers & Prevention.* 1998;7(12):1133-1144.

4. Boyd NF, O'Sullivan B, Campbell JE, et al. Mammographic signs as risk factors for breast cancer. *British Journal of Cancer.* 1982;45(2):185-193.

5. Byng JW, Yaffe MJ, Jong RA, et al. Analysis of mammographic density and breast cancer risk from digitized mammograms. *Radiographics.* 1998;18(6):1587-1598.

6. Warner E, Lockwood G, Tritchler D, Boyd NF. The Risk of Breast Cancer Associated with Mammographic Parenchymal Patterns: A Meta-Analysis of the Published Literature to Examine the Effects of Method of Classification. *Cancer Detection and Prevention.* 1992;16(1):67-72.

7. Wolfe JN. Breast patterns as an index of risk for developing breast cancer. *American Journal of Roentgenology.* 1976;126(6):1130-1137.

8. Wolfe JN. Breast parenchymal patterns and their changes with age. *Radiology.* 1976;121(3 Pt. 1):545-552.

9. Wolfe JN. Risk for breast cancer development determined by mammographic parenchymal pattern. *Cancer.* 1976;37(5):2486-2492.

10. Wolfe JN, Saftlas AF, Salane M. Mammographic parenchymal patterns and quantitative evaluation of mammographic densities: a case-control study. *AJR. American Journal of Roentgenology.* 1987;148(6):1087-1092.

11. Boyd NF, Lockwood GA, Martin LJ, Byng JW, Yaffe MJ, Tritchler DL. Mammographic density as a marker of susceptibility to breast cancer: a hypothesis. *IARC Scientific Publications.* 2001;154:163-169.

12. *The ACR Breast Imaging Reporting and Data System (BI-RADS) Atlas*. 3 ed. Reston, VA: American College of Radiology; 2003.

13. Niklason LT, Christian BT, Niklason LE, et al. Digital tomosynthesis in breast imaging. *Radiology.* 1997;205(2):399-406.

14. Conant EF, Schnall MD, Weinstein S. Multimodality screening for breast cancer in a high risk population. Paper presented at: RSNA, 2004; Chicago, IL.

15. Rafferty EA. Tomosynthesis: New Weapon in Breast Cancer Fight. *Decisions in Imaging Economics.* April 2004 2004;17(4).

16. Poplack S, Kogel C, Nagy H. Initial experience with digital breast tomosynthesis in 99 breasts of 98 women with abnormal digital screening mammography. Paper presented at: RSNA 2005; Chicago, IL.

17. Gail MH, Brinton LA, Byar DP, et al. Projecting individualized probabilities of developing breast cancer for white females who are being examined annually. *J Natl Cancer Inst.* 1989;81(24):1879-1886.

18. Claus EB, Risch N, Thompson WD. Autosomal dominant inheritance of early-onset breast cancer: Implications for risk prediction. *Cancer.* 1994;73(3):643-651.

19. Byng JW, Boyd NF, Fishell E, Jong RA, Yaffe MJ. The quantitative analysis of mammographic densities. *Physics in Medicine & Biology.* 1994;39(10):1629-1638.

20. Cerhan JR, Sellers TA, C.A. J, S. PV, K.R. B, C.M. V. Prenatal and perinatal correlates of adult mammographic breast density. *Cancer epidemiology, biomarkers, and prevention.* 2005;14(6):1502-1508.

21. Buist DSM, Aiello EJ, Miglioretti DL, White E. Mammographic Breast Density, Dense Area, and Breast Area Differences by Phase in the Menstrual Cycle *Cancer Epidemiology Biomarkers, and Prevention* 2006;15:2303-2306.

22. Vachon CM, Sellers TA, Vierkant RA, Wu F-F, Brandt KR. Case-Control Study of Increased Mammographic Breast Density Response to Hormone Replacement Therapy *Cancer Epidemiology, Biomarkers, and Prevention* 2002;11:1382-1388.

23. Khan QJ, Kimler BF, Smith EJ, O'Dea AP, Sharma P, Fabian CJ. Correlation of mammographic breast density with Ki-67 expression in benign breast epithelial cells obtained by random periareolar fine needle aspiration of high risk women *Journal of Clinical Oncology.* 2006;24(18S):1011.

24. Moré MJ, Narayanan D, Goodale PJ, Williams MB. Analysis of Spatial Correlation between 99mTc-Sestamibi Uptake and Radiographic Breast Density. *Technology in Cancer Research and Treatment.* 2005;4(3):265-273.

25. Harvey JA. Quantitative Assessment of Percent Breast Density: Analog Versus Digital Acquisition. *Technology in Cancer Research andTreatment.* 2004;3(6):611-616.

26. Lundström E, Söderqvist G, Svane G, et al. Digitized assessment of mammographic breast density in patients who received low-dose intrauterine levonorgestrel in continuous combination with oral estradiol valerate: a pilot study. *Fertility and Sterility.* 2006;85(4):989-995.

27. Mitchell G, Antoniou AC, Warren R, et al. Mammographic Density and Breast Cancer Risk in BRCA1 and BRCA2 Mutation Carriers *Cancer Research* 2006;66:1866-1872.

28. Saha PK, Udupa JK, Conant EF, Chakraborty DP, Sullivan D. Breast tissue density quantification via digitized mammograms. *IEEE Transactions on Medical Imaging.* 2001;20(8):792-803.

29. Marias K, Behrenbruch C, Highnam R, Parbhoo S, Seifalian A, Brady M. A mammographic image analysis method to detect and measure changes in breast density. *European Journal of Radiology.* 2004;52(3):276-282.

30. Shepherd JA, Kerlikowske KM, Smith-Bindman R, Genant HK, Cummings SR. Measurement of breast density with dual x-ray absorptiometry: feasibility. *Radiology.* 2002;223:554-557.